ALMA Memo. 416

The Relative Sensitivity of Full-Wave and Half-Wave Detectors in Radio Astronomy

A. R. Thompson and D. T. Emerson
National Radio Astronomy Observatory

3 April, 2002

Abstract

The sensitivity in the measurement of Gaussian noise power using a half-wave detector can suffer degradation relative to that of a full-wave detector, in cases where the bandwidth of the input waveform is not small compared to the center frequency. There are two physical mechanisms that suggest a basis for this effect. The half-wave detector responds to only half of the input waveform, resulting in possible loss of information. Also, in the half-wave detector a component of the input spectrum feeds through the diode and adds to the noise that is subsequently filtered by averaging at the detector output. This feedthrough component does not occur in full-wave detectors. The phenomena are examined using an analytic method developed by Nuttall (1986), and also by numerical simulation. The results for both linear and square-law characteristics are considered, and formulas and graphs for estimating the magnitudes of the effects are given.

It has generally been assumed that in measuring the power level in a radio astronomy receiver, use of a half-wave detector provides the same sensitivity (i.e. signal-to-noise ratio) as a full-wave detector [1]. This is certainly true for cases where the bandwidth of the input to the detector is small compared with the center frequency, but increasing use of broadband systems has led to the use of IF amplifiers with baseband (lowpass) responses. There are two considerations which indicate that with such baseband responses the signal-to-noise ratio obtained with a half-wave detector could be less than with a full-wave one: firstly the loss of effective integration time, and secondly the component of the input spectrum that occurs at the output of the diode.

Loss of integration time

The half-wave detector makes use of the input signal for only half of the time, so unless the negative part of the signal is 100% correlated with the positive part, there will be an effective loss of integration time. For the case of a band limited signal that is sampled at the Nyquist rate, and where, say, all the negative samples are thrown away before a numerical detection process, the effect is easy to predict. For Nyquist sampling all samples are statistically independent. If all negative samples are deleted, then almost exactly half of the independent data are being ignored. The effective integration time will be halved, with an anticipated $\sim\sqrt{2}$ loss of signal-to-noise ratio. For detection of data that have not first been sampled, the

[1] A full-wave detector can be envisaged as a pair of half-wave detectors in which the polarity of one diode is reversed with respect to the other. The input signal is fed through a power splitter to the two detector inputs and the outputs drive the two inputs of a differencing amplifier.

analysis is more complicated. The gaps where the signal is ignored in half-wave detection have an average duration of approximately half a cycle at the IF center frequency. The autocorrelation function of the input noise waveform falls substantially over a time interval equal to the reciprocal of the signal bandwidth, which for a baseband spectrum is approximately equal to the average half-wave gap length. Thus, for baseband spectra, adjacent positive and negative parts of the waveform are not 100% correlated and the information rejected by the half-wave detector may not be entirely redundant–hence, again, a potential loss of effective integration time.

Feedthrough of unmodified input

A fundamental difference between the actions of a half-wave and a full-wave detector is that in the half-wave detector a component of the input spectrum that is not modified by the detection process appears at the output of the diode, and is then time-averaged along with the detected components. We refer to this component as the feedthrough component. During the intervals that the diode is conducting, frequency components of the input waveform pass through it. In a half-wave detector these are all processed by the time-averaging stage, but in a full-wave detector the feedthrough components from the two diodes cancel one-another. Intuitively this difference between full-wave and half-wave detection can also be seen by considering the Fourier components of a full-wave and a half-wave rectified sine wave of frequency f. After half-wave rectification there are frequency components 0, f, $2f$, $4f$, $6f, \ldots$. After full-wave rectification there are only components at frequencies 0 and even multiples of f, i.e. there is no component at f. If the spectrum of the input signal extends down to sufficiently low frequencies the feedthrough component will appear as additional noise, indistinguishable from the inherent noise in the detected signal, and so will result in a degradation of the half-wave signal-to-noise ratio.

Spectral overlap

Figure 1 shows the spectrum of the input to the detector, for which we use a rectangular model, and the frequency response of the averaging process at the output of the detector. Fridman (1997) has considered the first of the two effects mentioned above, that is, the loss of nonredundant data or the effective loss of integration time, but our results do not support his analysis. A detailed analysis of the response of half- and full-wave detectors is given in an extensive report by Nuttall (1986). In this memorandum we present results using both Nuttall's method and numerical simulation. We are concerned mainly with detectors with a square-law response since this provides the best signal-to-noise ratio in radiometry (Kelly, Lyons, and Root 1963), but for comparison we also include the linear detector.

Analysis Using Nuttall's Method

The input to the detector is an IF waveform $x(t)$ with Gaussian probability distribution and a rectangular power spectrum of width W. The low frequency cutoff of the spectrum is at f_L. We first consider square-law detection, that is, the output of the detector before averaging is $y(t) = x^2(t)$. Note that x takes the range $-\infty$ to ∞ for the full-wave detector and zero to ∞ for the half-wave detector. The output is $y(t)$ averaged with uniform weighting over time interval T, that is, $z(t) = \int y(\tau)h(t-\tau)d\tau$, where $h(t)$ is the impulse response of the averaging filter. To determine the relative sensitivities of the full-wave and half-wave systems we need to determine the mean and variance of $z(t)$ for each case.

To determine the output variance σ_z^2 we need the autocorrelation function of $y(t)$, which is

$$R_y(\tau) = \overline{y(t)y(t-\tau)} = \iint g(x_a)g(x_b)\, p_2(x_a, x_b, \tau)dx_a\, dx_b, \tag{1}$$

where the bar denotes an average, $g(x)$ is the nonlinearity characteristic of the detector and is equal to $|x|$ for a linear detector and x^2 for a square-law detector, and p_2 is the second-order probability density function

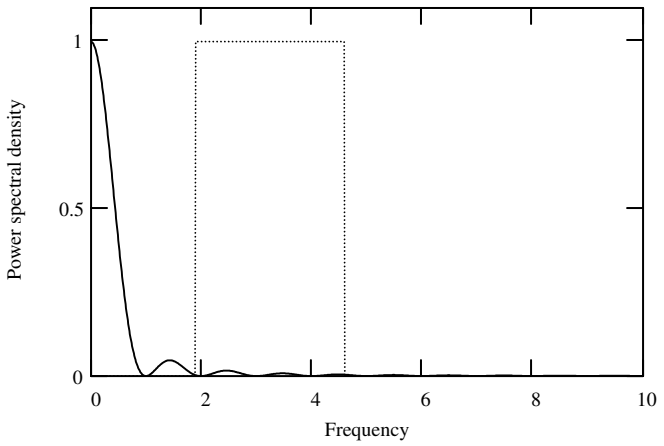

Figure 1: The full curve is the sinc-squared function $\left[\frac{\sin(\pi f T)}{(\pi f T)}\right]^2$, where f represents frequency. This is the response at the detector output resulting from averaging with uniform weight for time T. The first zero in the function occurs at frequency T^{-1}. The broken curve shows the rectangular passband used to represent the spectrum of the input signal. The frequency of the lower edge of the passband is f_L and the bandwidth is W. The fractional frequency offset of the band from a true baseband response is f_L/W.

of the input $x(t)$. Barrett and Lampard (1955) show that p_2 can be written as

$$p_2(x_a, x_b, \tau) = p_1(x_a)p_1(x_b)\sum_{k=0}^{\infty}\frac{1}{k!}\rho^k(\tau)\mathrm{He}_k\Big(\frac{x_a}{\sigma_x}\Big)\mathrm{He}_k\Big(\frac{x_b}{\sigma_x}\Big), \tag{2}$$

where $\rho(\tau)$ is the normalized autocorrelation function of $x(t)$, $\mathrm{He}_k(x)$ is the Hermite polynomial of degree k, and p_1 is the first-order probability function:

$$p_1(x) = \frac{1}{\sqrt{2\pi}\sigma_x}e^{-(x^2/2\sigma_x^2)}. \tag{3}$$

Substituting Eq. (2) into Eq. (1) yields

$$R_{\bar{y}}(\tau) = \sum_{k=1}^{\infty}\frac{1}{k!}\rho^k(\tau)\Big[\int g(x)p_1(x)\mathrm{He}_k\Big(\frac{x}{\sigma_x}\Big)dx\Big]^2, \tag{4}$$

In Eq. (4) the term for $k = 0$, which is equal to the mean squared value of $y(t)$, is omitted. Thus $R_{\bar{y}}$ is the autocorrelation of the zero-mean detected waveform before averaging. The variance of the output after averaging is

$$\sigma_z^2 = \int_{-T}^{T} R_{\bar{y}}(\tau)a(\tau)d\tau, \tag{5}$$

where $a(\tau)$ is the autocorrelation of the impulse response of the averaging process.

For the half-wave square-law detector we consider the case where the diode conducts when the input signal voltage is positive. Then the limits of the integral within the square brackets in Eq. (4) are 0 to ∞. We consider the case where the input waveform is sampled at time intervals Δ, for which we use a value small compared with the reciprocal bandwidth of the input to simulate the response of an analog system.

The integral is evaluated by summation and Eq. (5) becomes

$$\sigma_{z\,HW}^2 = \frac{\sigma_x^4}{4}\sum_{k=1}^{\infty} U(k) \sum_{n=-M}^{M} \Big(1 - \frac{|n|}{M}\Big)\rho^k(n\Delta), \tag{6}$$

where the factor $\sigma_x^4/4$ is the square of the expectation of the mean of $y(t)$ and $\big(1 - \frac{|n|}{M}\big)$ represents the autocorrelation function of the averaging process. M is the number of samples in time T. $U(k)$ is a function that incorporates the integral in Eq. (4) and is defined in the Appendix, in which a recurrence formula and starting values are given from which $U(k)$ can be evaluated. For the square-law detector $U(k) = 0$ for $k \geq 4$ and $U(2) = 2$. Thus from Eq. (6)

$$\sigma_{z\,HW}^2 = \frac{\sigma_x^4}{4}\Bigg[2\sum_{n=-M}^{M}\Big(1 - \frac{|n|}{M}\Big)\rho^2(n\Delta) + \sum_{k=1\,(odd)} U(k) \sum_{n=-M}^{M}\Big(1 - \frac{|n|}{M}\Big)\rho^k(n\Delta)\Bigg], \tag{7}$$

and using $\sum_{k=1\,(odd)}^{\infty} U(k) = 3$ (see the Appendix) we obtain,

$$\sigma_{z\,HW}^2 = \frac{\sigma_x^4}{4}\Bigg[5 + 4\sum_{n=1}^{M}\Big(1 - \frac{n}{M}\Big)\rho^2(n\Delta) + 2\sum_{k=1\,(odd)}^{\infty} U(k) \sum_{n=1}^{M}\Big(1 - \frac{n}{M}\Big)\rho^k(n\Delta)\Bigg]. \tag{8}$$

For the full-wave detector the limits of the integral within square brackets in Eq. (4) are $\pm\infty$. Since He_k is odd for odd values of k, it follows that the integral is zero for odd values of k. Thus we consider only $k = 2$ and from Eq. (5) obtain

$$\sigma_{z\,FW}^2 = \sigma_x^4\Bigg[2 + 4\sum_{n=1}^{M}\Big(1 - \frac{n}{M}\Big)\rho^k(n\Delta)\Bigg]. \tag{9}$$

The ratio of the sensitivities (signal-to-noise ratios) of the half-wave (HW) and full-wave (FW) detectors is

$$\frac{SNR_{FW}}{SNR_{HW}} = 2\sqrt{\frac{\sigma_{z\,HW}^2}{\sigma_{z\,FW}^2}}, \tag{10}$$

where the factor of 2 on the right-hand side occurs because the signal voltage at the output of the full-wave detector is twice that for the half-wave one. From Eqs. (8)-(10) the sensitivity ratio is

$$\frac{SNR_{FW}}{SNR_{HW}}\Big|_{SQL} = \Bigg[\frac{5 + 4\sum_{n=1}^{M}(1 - \frac{n}{M})\rho^2(n\Delta) + 2\sum_{k=1\,(odd)}^{\infty} U(k)\sum_{n=1}^{M}(1 - \frac{n}{M})\rho^k(n\Delta)}{2 + 4\sum_{n=1}^{M}\big(1 - \frac{n}{M}\big)\rho^2(n\Delta)}\Bigg]^{1/2}. \tag{11}$$

Following the same procedure, we also obtain the sensitivity ratio for linear detectors:

$$\frac{SNR_{FW}}{SNR_{HW}}\Big|_{LIN} = \Bigg[\frac{\pi - 1 + \pi\sum_{n=1}^{M}(1 - \frac{n}{M})\rho(n\Delta) + 2\sum_{k=2\,(even)}^{\infty} U(k)\sum_{n=1}^{M}(1 - \frac{n}{M})\rho^k(n\Delta)}{\frac{\pi}{2} - 1 + 2\sum_{k=2\,(even)}^{\infty} U(k)\sum_{n=1}^{M}\big(1 - \frac{n}{M}\big)\rho^k(n\Delta)}\Bigg]^{1/2}. \tag{12}$$

Here the $U(k)$ terms are different from those for the square-law case; see the Appendix. For the spectrum of the input waveform $x(t)$ we use as a model a rectangular function with bandwidth W and center frequency $(f_L + \frac{1}{2}W)$. The fractional frequency offset of the input band from a true baseband spectrum is f_L/W. Thus the autocorrelation function ρ is

$$\rho(n\Delta) = \frac{\cos[2\pi(\frac{f_L}{W} + \frac{1}{2})Wn\Delta]\sin(\pi Wn\Delta)}{\pi Wn\Delta}. \tag{13}$$

Curves of the sensitivity ratio as a function of f_L/W from Eqs. (12) and (13)are shown in Fig. 2. In the calculations we use Δ equal to 1/20 of the reciprocal bandwidth, i.e. $W\Delta = 1/20$. Within time T there are M samples, so $T = M\Delta$, and $TW = M/20$. An upper limit of 49 for k is satisfactory. Figure 2 shows the ratio SNR_{FW}/SNR_{HW} as a function of f_L/W for $TW = 16$ and 160, using $M = 320$ and 3200 respectively. For $f_L/W = 0$ the sensitivity ratio shows a small variation (a few percent) with TW, and for $TW = 16$ is equal to 1.99 for the linear detector and 1.57 for the square-law one. Each of the three curves approaches unity in two parts: a rapid fall-off, followed by a relatively slow one. Comparison of the first parts for the two curves for the square-law detector indicates that the rate of fall-off is inversely proportional to the averaging time T. For $TW = 160$ the rapid fall-off is complete at $f_L/W \approx 0.05$. The range of the rapid drop off is $f_L = 0$ to $f_L \approx 0.8/T$, that is, the range in which the low-frequency cutoff of the IF bandpass is less than the frequency of the first zero in the sinc-squared response of the averaging process. This is consistent with the expected behavior for the second of the two mechanisms mentioned earlier (feedthrough of IF components). The slow fall-off can similarly be explained, in part, by the response to the tail of the sinc-squared function resulting from the averaging. Note that for linear detection the amplitude of the slow fall-off component is smaller than that for the square-law case with the same value of TW.

Numerical simulation

To provide an independent analysis, and to investigate further the processes involved in the detector action, a numerical simulation was performed. The simulated data set consists of one million (2^{20}) random numbers with normal, or Gaussian, probability distribution. A Fourier transform was performed on the entire set of 10^6 data points. The transformed array was then zero-padded, such that after an inverse Fourier transform a new data set of 8×10^6 points was derived, equivalent to the original raw data but now 8:1 oversampled. Further, the original 10^6 points were split into two independent arrays of 5×10^5 points, each of which, by means of a Fourier transform, zero padding and inverse Fourier transform, were turned into two statistically independent arrays of 8×10^6 points, now oversampled by 16:1. Simultaneously a Fourier transform was used to obtain a quadrature version of the same data.

To obtain a baseband-shifted version of the same random, oversampled data, an image rejection (single sideband) mixer was simulated, using these real and quadrature sets of random data with a cosine and a sine representation of the local oscillator. This enabled a baseband noise signal to be shifted up in frequency by any amount consistent with the 8:1 or 16:1 oversampling rates, including frequency shifts by very small fractions of the baseband bandwidth, without concern for overlapping mixer products. This particular single-sideband frequency shifting process was computationally very efficient.

Subsequent analysis was performed with each or these 16:1 and 8:1 oversampled data sets, with a variety of baseband frequency shifts. Both half- and full-wave detection, using both linear and square-law characteristics, were applied to the data set. Averaging with uniform weighting over time T then allowed the variance of the noise at the detector outputs to be estimated. Figure 3 shows an example of curves for the sensitivity ratio for square-law detection as a function of f_L/W. In all cases the results are in good agreement with those obtained by Nuttall's method.

The numerical simulation also allows examination of the spectrum of $y(t)$ before the final averaging process, by means of Fourier transformation of the data at that point. Figure 4 shows an example of such spectra for linear detection; as expected, the rectangular input spectrum has produced, after detection, a triangular power spectrum at baseband, and a symmetric triangular spectrum of lower peak amplitude at twice the input frequency. Note that for half-wave detection a component of the rectangular input spectrum feeds through the diode, but does not appear in the full-wave case. The contribution of this feedthrough component to the variance at the detector output is proportional to the response of the averaging process integrated over the input passband. For averaging with uniform weight over time T the power response is proportional to the sinc-squared function $[\sin(\pi Tf)/(\pi Tf)]^2$. Thus, for the linear half-wave detector the

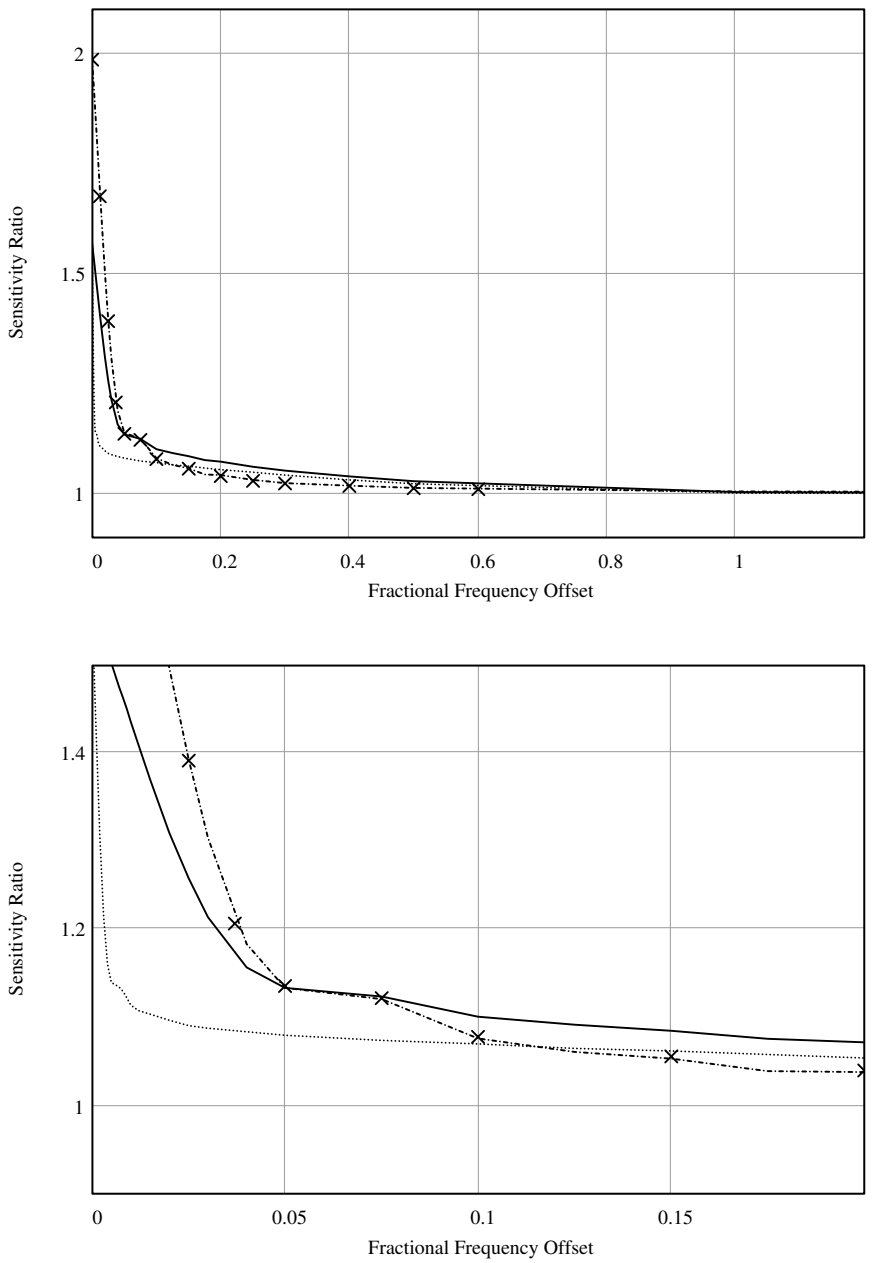

Figure 2: The ordinate in both panels is the sensitivity ratio calculated using Nuttall's method. The full curve is for square-law detectors with $TW = 16$. The dotted curve is for square-law detectors with $TW = 160$. The dash-dot curve is for linear detectors with $TW = 16$. The crosses indicate values of the sensitivity ratio for linear detectors from Eq. (15).

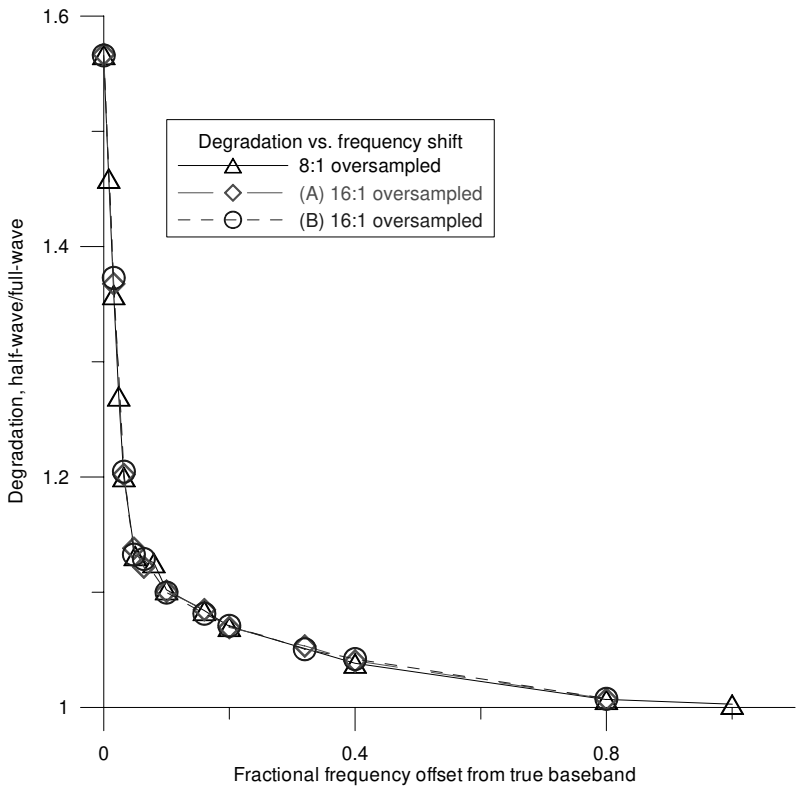

Figure 3: The ordinate is the sensitivity ratio for square-law detectors with $TW = 16$ and the abscissa is the fractional frequency offset from a true baseband response. Triangular points indicate the data set with 8:1 oversampling and circular and diamond-shaped points indicate the two data sets with 16:1 oversampling. Note the good agreement between the results for the three data sets and between these results and the full curve in Fig. 2.

contribution to the output variance is proportional to

$$2T \int_{f_L}^{f_L+W} \left(\frac{\sin(\pi T f)}{\pi T f} \right)^2 df. \tag{14}$$

This expression has been normalized so that the integral is equal to unity when the limits are 0 and ∞. At $f_L = 0$ the data in Figs. 2 and 3 indicate that for the linear detector the variance of the half-wave output exceeds that of the full-wave output by a factor $1.99^2 = 3.96$. Thus the in half-wave case a component of variance 2.96 times that of the full wave variance has been added to the output. The sensitivity ratio to be expected as a result of the feedthrough component is

$$\left. \frac{SNR_{FW}}{SNR_{HW}} \right|_{LIN} = \sqrt{1 + 2.96 \times 2T \int_{f_L}^{f_L+W} \left[\frac{\sin(\pi T f)}{\pi T f} \right]^2 df}. \tag{15}$$

Points derived from this equation for $TW = 16$ are shown as crosses in Fig. 2 and these agree with the curve derived from Eq. (12) with an accuracy of $\sim 0.5\%$ or better.

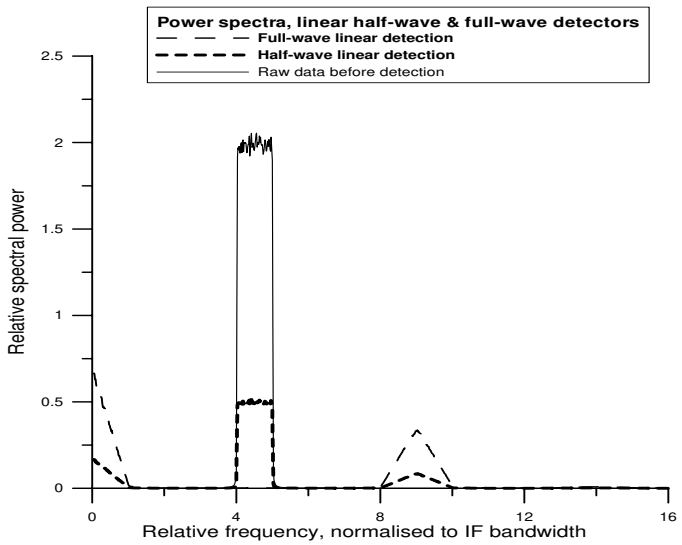

Figure 4: The full line shows the input spectrum, and the broken lines the detected output (before time-averaging), for half-wave (bold line) and full-wave square-law detection. The abscissa is frequency. For half-wave detection the input spectrum feeds through the diode at a level of 1/4 the input power. Note that this is the same ratio as the powers of the corresponding components in the case of a half-wave rectified sine wave. For full-wave detection no such feedthrough occurs. The data are from numerical analysis.

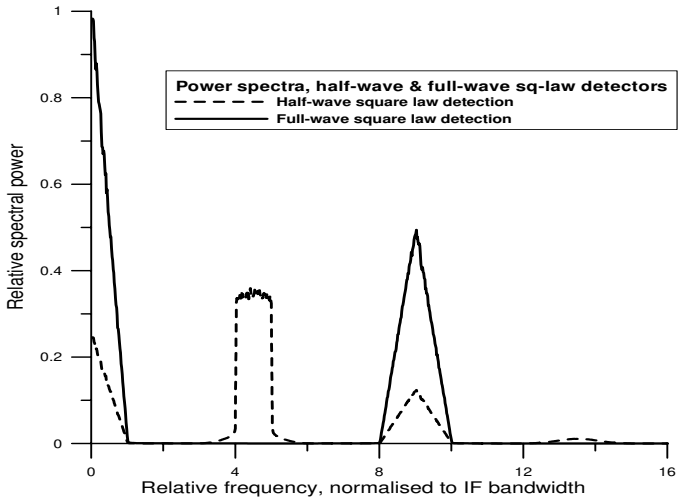

Figure 5: The full line shows the output spectrum (before time-averaging) for a full-wave square-law detector and the broken line shows the same function for a half-wave square-law detector. The input is not shown but is the same as in Fig. 4. For the half-wave detector there is again a feedthrough component within the input frequency band, but in this case the component has acquired low-level "wings" that extend over a range of frequency equal to three times the input bandwidth. The amplitude scale has been increased relative to that of Fig. 4 to emphasize these details. The spectral wings do not occur in the linear half-wave case.

For the square-law case, the power spectrum of the detected signal before time averaging is shown in Fig. 5. Again there is a feedthrough component, but in this case it is modified by the squaring of the amplitude which produces the spectral "wings" at the base of the rectangular feedthrough seen in Fig. 5. The amplitude of these wings is proportional to the square of the distance from the tip of the wing. This feature evidently results from part of the rectangular feedthrough spectrum becoming convolved with the triangular responses centered at zero frequency and at the second harmonic. That is, the profile of the wings results from the convolution of a rectangle of width W with a triangle of base width $2W$, which produces a component with a base width of $3W$ centered on the input band. The wings therefore have a parabolic profile and extend for a distance W on either side of the input band. The relative amplitude of the component resulting from this convolution is small, but the wing on the low-frequency side of the input band can have a significant effect on the detector output if it extends into the frequency range below $1/T$, where the major response of the time averaging function occurs. Thus, to obtain an expression for the sensitivity ratio for square-law detectors based on the spectrum in Fig. 5, it is necessary to consider the response to the low-frequency wing as well as to the feedthrough in the rectangular passband. The response to the rectangular component is the same as in Eq. (15), except that for the square-law case the factor 2.96 is replaced by $1.57^2 - 1 = 1.46$. For the low-frequency wing the resulting variance after time averaging is proportional to

$$2T \int_{f_L - W}^{f_L} \left[\frac{\sin(\pi T f)}{\pi T f}\right]^2 \left(\frac{W - f_L + f}{W}\right)^2 df. \tag{16}$$

This can be combined with the response to the feedthrough within the rectangular passband to give

$$\left.\frac{SNR_{FW}}{SNR_{HW}}\right|_{SQL} \simeq \sqrt{1 + 1.46\left\{2T \int_{f_L}^{f_L + W} \left[\frac{\sin(\pi T f)}{\pi T f}\right]^2 df + 0.06 \times 2T \int_{f_L - W}^{f_L} \left[\frac{\sin(\pi T f)}{\pi T f}\right]^2 \left(\frac{W - f_L + f}{W}\right)^2 df\right\}}, \tag{17}$$

where the factor 0.06 represents the spectral density of the wing component relative to that of the feedthrough within the input band, as determined by the numerical analysis. Figure 6 shows an example of how the two components in Eq. (16) combine to form a curve that is in good agreement with the corresponding points derived using Nuttall's method. Thus we conclude that the feedthrough components in the half-wave detector, as modified buy the power-law characteristic, provide a physical basis that accurately describes the relative sensitivity of half- and full-wave detectors.

Note that in Figs. 4 and 5 the ratio of the output spectral noise powers for full-wave and half-wave detectors, for frequencies near zero, is 4:1. The signal power outputs have the same ratio since the full-wave signal amplitude is twice the half-wave amplitude. Thus in cases where the output noise results solely from the triangular components near zero frequency, that is, cases where the center frequency of the IF is sufficiently larger than the bandwidth, the signal to noise ratio is the same for both full-wave and half-wave detectors.

Sensitivity ratio for large Averaging-Time–Bandwidth product

In radio astronomy, values of T ~1 s and W ~1 GHz resulting in TW values as high as 10^9 are commonly used. For such large values of TW, evaluation of the sensitivity ratio by Nuttall's method, or by numerical analysis, results in large computing loads. However, the approach used in Eqs. (15) and (17) can be adapted for estimation of the sensitivity ratio in this case. In general, the sensitivity ratio depends upon three parameters, T, W, and f_L. For large TW, however, each of the integrals involved depends principally on only two parameters. In the case of the response to the feedthrough within the rectangular passband, we can let the upper band-edge frequency tend to infinity since the sinc-squared averaging function ensures that the integral in Eq. (15) and the first integral in Eq. (17) will converge. Thus only T and f_L are involved and

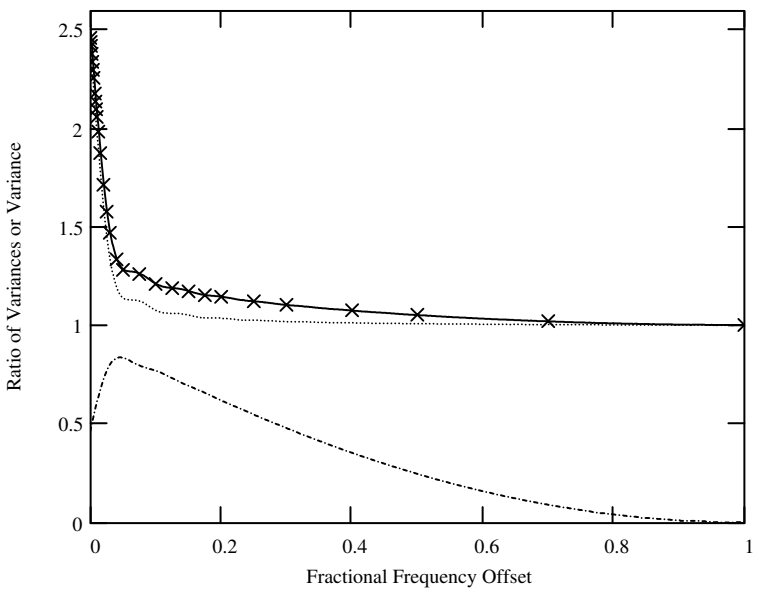

Figure 6: For the top two curves, the ordinate is the square of the sensitivity ratio (i.e. the ratio of the variances rather than the signal-to-noise ratios). The abscissa is the fractional frequency offset of the input band from a true baseband response, that is, f_L/W. All data are for square-law detectors with $TW = 16$. The dotted line is the response to the feedthrough component within the rectangular passband as given by the first integral under the square root sign in Eq. (17). The dash-dot curve is the response to the wing component from expression (16), and here the ordinate is the variance. The full line is the dotted curve plus 0.06 times the response to the wing, i.e. the expression under the square root in Eq. (17). The crosses are points calculated by Nuttall's method.

for the linear detector we have:

$$\left.\frac{SNR_{FW}}{SNR_{HW}}\right|_{LIN} \simeq \sqrt{1 + 2.96A(Tf_L)}, \tag{18}$$

where $A(Tf_L) = 2\int_{Tf_L}^{\infty}\left[\frac{\sin(\pi x)}{\pi x}\right]^2 dx$ and x is a dummy variable of integration. A graph of this function is shown in Fig. 7. For the response to the wing component in the square-law case, large TW implies that the frequency interval over which the sinc-squared function is significantly greater than zero is small compared with the length of the wing. Since the area under the sinc-squared function is normalized to unity, the response is not dependent on T so long as TW has a value approaching 100, or more. Thus for square-law detectors we have:

$$\left.\frac{SNR_{FW}}{SNR_{HW}}\right|_{SQL} \simeq \sqrt{1 + 1.46[A(Tf_L) + 0.12B(f_L/W)]}, \tag{19}$$

where $B(f_L/W) = [1 - (f_L/W)]^2$ for $0 < f_L/W < 1$ and is zero otherwise; this provides an approximation for the response to the wing component. From Fig. 7, $A(Tf_L)$ falls to 10^{-2} for $Tf_L = 10$ and 10^{-3} for $Tf_L = 100$. For example, if $T = 1$ s, these values correspond to $f_L = 10$ Hz and 100 Hz respectively. Now suppose that $f_L = 100$ Hz and the bandwidth W is 10 MHz. Then $f_L/W = 10^4$, so $B(f_L/W) \simeq 1$ and the sensitivity ratio is 1.08. Thus, unless Tf_L is less than ~ 10, the A term is negligible and the degradation of the half-wave sensitivity results from the B term, which only approaches zero when $f_L \simeq W$ or greater,

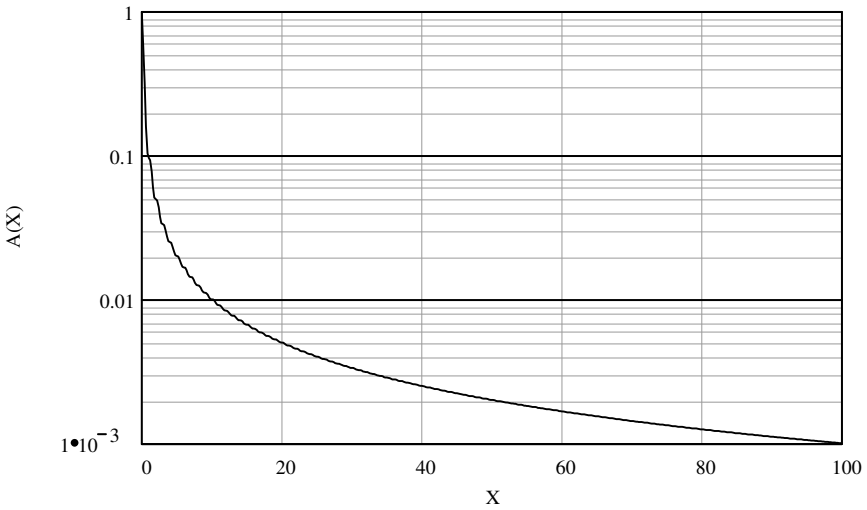

Figure 7: The ordinate is $A(X) = 2\int_X^\infty \left[\frac{\sin(\pi x)}{\pi x}\right]^2 dx$, for evaluation of $A(Tf_L)$. The ripples in the curve result from the reduction in slope as the lower level of the integral passes through zeros in the sinc-squared function.

that is when the wing component no longer extends into the main part of the response in the sinc-squared averaging function. Thus, there can be conditions when the sensitivity ratio is essentially unity for linear detectors but as high as 1.08 for square-law detectors. However, Nuttall (1986) shows that for small signal to noise ratios, the sensitivity of square-law detectors is greater than that of linear detectors by a factor of 1.07, so the advantage that the linear detector offers in these particular conditions is negligible.

Discussion

In considering the physical interpretation of the results it is useful to start with the simple case of Nyquist sampling, in which the samples are uncorrelated [i.e., $\rho(n\Delta) = 0$]. This occurs for a the sampling rate equal to twice the bandwidth [i.e., $\Delta = 1/(2W)$] and also requires that the fractional frequency offset be an integer. The variances of the outputs for square-law, half-wave and full-wave detectors (for the same output signal strength) are represented by the numerator and denominator, respectively, of the expression in square brackets on the right-hand side of Eq. (11). For Nyquist sampling this ratio of variances is 5/2, resulting in a sensitivity ratio of $\sqrt{2.5} = 1.58$. As Fridman (1998) points out, the mean and mean-squared values of $y(t)$ for a full-wave square-law detector are equal to σ_x^2 and $3\sigma_x^4$, respectively. The variance of $y(t)$ is equal to the mean-squared value minus the square of the mean, that is, $2\sigma_x^4$. For a half-wave square-law detector the mean and mean-squared values of $y(t)$ are half those for the full-wave case, resulting in a variance of $1.25\sigma_x^4$ and a sensitivity ratio of $\sqrt{2.5}$, in agreement with Eq. (11). Note that if the zeros inserted when the diode does not conduct were removed from the $y(t)$ sequence for a half-wave detector, the mean and mean squared values would be the same as in the full-wave case, but the length of the sequence would be halved. Thus $\sqrt{2}$ of the relative sensitivity factor 1.58 can be attributed to loss of half the data, and the remainder to the fact that the zeros are processed as valid data in the averaging stage. However, Nyquist sampling does not apply to the general usage of a detector in which the input is a continuous analog voltage. To simulate the continuous case we used 10 times the Nyquist rate [i.e. $\Delta = 1/(20W)$] in using Nuttall's method, and 8 or 16 times the Nyquist rate in numerical analysis.

A basic difference in performance between half- and full-wave detectors is that in the half-wave case a

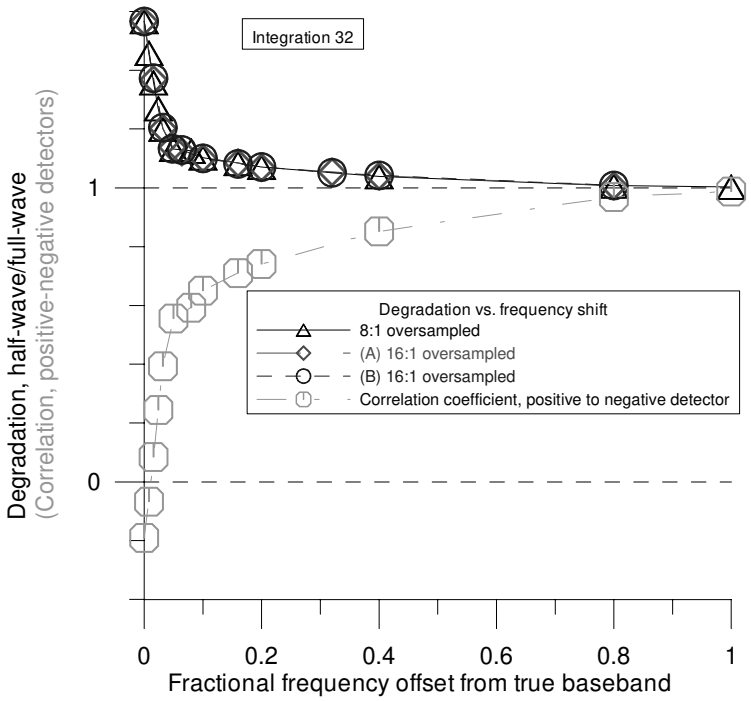

Figure 8: The top curve shows the sensitivity ratio (degradation of the half-wave detector sensitivity) for square law detectors with $TW = 16$. The lower curve shows the correlation of the positive and negative values of the input samples, that is the correlation of the date that are used and the data that are ignored in a half-wave detector, again for a square-law response with $TW = 16$.

component of the input spectrum feeds through the diode to the averaging stage and can add to the variance at the output. In the full-wave detector this does not occur. To examine the question of whether the data that are ignored in half-wave detection are correlated with those that are accepted, numerical simulation was used to determine the cross correlation between the outputs of two half-wave detectors with diodes of opposite polarity and a common input waveform. The result is shown in Fig. 8 for TW=16 where it is compared with the sensitivity ratio for square-law detectors. The cross correlation starts with a negative value when the frequency offset of the input band is zero, at which point the sensitivity ratio is 1.57. The cross correlation then increases to unity (i.e., the detector outputs become fully correlated) as the sensitivity ratio approaches unity. Note that, as would be expected, the sensitivity ratio is $\sqrt{2}$ at the offset value for which the cross correlation is zero. The negative correlation at small offsets results in part from the fact that the fraction of input samples that are positive and the fraction that are negative are not exactly equal, but sum to unity, and thus are negatively correlated. The suggestion that the half-wave detector loses sensitivity by ignoring nonredundant data gains some support from Fig. 8, but as an alternate way of viewing the effect of the input feeding through the diode rather than as a separate mechanism.

For continuum observations the sensitivity of radio astronomical measurements is proportional to the square root of the bandwidth accepted by the receiver. However, with IF bandwidths of megahertz or more, extending the low end of the bandpass below ∼100 Hz does not significantly increase the sensitivity, but risks introducing 60 Hz power line pickup and other low frequency noise. Thus broadband IF amplifiers rarely extend to such low frequencies, and overlap with the frequency response of the time averaging process

does not usually arise. There remains the effect of the response to the wing component in half-wave square-law detectors. This produces a maximum degradation of approximately 8% in the signal-to-noise ratio when the frequency offset is small. For fractional frequency offsets of 0.1, 0.2, 0.5, and 0.8 the degradation values are approximately 7%, 5%, 2%, and <0.5%, from Eq. (19) for the case where $A(Tf_L)$ is negligible. Although this loss is small, it may be considered expensive if compared with the effective loss of area of a large radio telescope. However, in parallel with the development of wide-band lowpass amplifiers there have been developments in high-speed digital processing, which result in the replacement of detectors by digital correlators which are inherently full-wave devices. In large instruments correlators are generally used to provide the main response of the system, but detectors continue to be used in small instruments and for monitoring purposes in large ones. For ALMA the first IF extends from 4 to 12 GHz, a fractional frequency offset from baseband of 0.5. From Eq. (19), with $Tf_L \geq 100$, it is seen that a half-wave square-law detector on this band would suffer a degradation of approximately 2% in signal-to-noise ratio relative to full-wave detector. However, in the ALMA design this first IF band is then split into four bands each covering 2–4 GHz, for which the baseband offset is 1.0 and the degradation has become negligible ($< 0.5\%$). Similarly for the EVLA the IF responses are 1–2 and 2–4 GHz, so again the fractional frequency offset is 1.0 and there should be no degradation with a half-wave square-law detector.

Acknowledgments. We wish to thank L. R. D'Addario, C. R. Masson, A. H. Nuttall, and F. R. Schwab for helpful discussions.

Appendix

The following details are from Nuttall (1986). $U(k)$ is defined as

$$U(k) = \frac{L^2(k)}{L^2(0)k!} \quad \text{for } k \geq 0, \tag{20}$$

where $L(0) = 1/\sqrt{2\pi}$ for linear detectors, $L(0) = 1/2$ for square-law detectors, and

$$L(k) = \int_0^\infty \frac{w^2}{\sqrt{2\pi}} e^{-w^2/2} \mathrm{He}_k(w) dw \quad \text{for } k \geq 0. \tag{21}$$

Values of $U(k)$ can be determined from the following recurrence formula,

$$U(k) = U(k-2)\frac{(q+2-k)^2}{k(k-1)} \quad \text{for } k \geq 2, \tag{22}$$

where q is the power law exponent, that is, 1 for a linear detector, and 2 for a square law detector. Starting values are $U(0) = 1$ (for all values of q) and

$$U(1) = \frac{2\Gamma^2(\frac{q}{2}+1)}{\Gamma^2(\frac{q+1}{2})}, \tag{23}$$

where Γ is the gamma function. Thus $U(1)$ is equal to $\pi/2$ for $q = 1$ and $8/\pi = 2.5465$ for $q = 2$. A further useful relationship is

$$\sum_{k=0\,(even)}^{\infty} U(k) \;=\; \sum_{k=1\,(odd)}^{\infty} U(k) \;=\; \frac{\pi^{1/2}\Gamma^2(\frac{q}{2}+1)}{\Gamma^2(\frac{q+1}{2})}, \tag{24}$$

that is, $\pi/2$ for $q = 1$ and 3 for $q = 2$.

References

Barrett, J. F. and D. G. Lampard, An Expansion of Some Second-Order Probability Distributions and its Application to Noise Problems, *IRE Trans. Inform. Theory*, **IT-1**, 10–15, 1955.

Fridman, P. A., Full-Wave Detection Against Half-Wave Detection in Radiometry, *Electronics Letters*, **34** No. 1, 1998.

Kelly, E. J., D. H. Lyons, and W. L. Root, The Sensitivity of Radiometric Measurements, *J. Soc. Indust. Appl. Math.*, **11**, 235–257, 1963.

Nuttall, A. H., *Signal-to-Noise Ratio Requirements for Half-Wave and Full-Wave Nonlinear Detectors with Arbitrary Power Laws, Sampling Rates, Input Spectra, and Filter Characteristics*, Technical Report 7633, Naval Underwater Systems Center, Newport, Rhode Island, 10 June 1986.